Basidiomycete-specific *PsCaMKL1* encoding a CaMK-like protein kinase is required for full virulence of *Puccinia striiformis* f. sp. *tritici*

Min Jiao[1,#], Dan Yu[2,#], Chenglong Tan[1], Jia Guo[1], Dingyun Lan[1], Ershang Han[1], Tuo Qi[1], Ralf Thomas Voegele[3], Zhensheng Kang[1], Jun Guo[1,*]

[1] State Key Laboratory of Crop Stress Biology for Arid Areas, College of Plant Protection, Northwest A&F University, Yangling 712100, Shaanxi, P. R. China

[2] College of Forestry, Northwest A&F University, Yangling 712100, Shaanxi, P. R. China

[3] Department of Phytopathology, Institute of Phytomedicine, Faculty of Agricultural Sciences, University of Hohenheim, 70599 Stuttgart, Germany

[#] These authors contributed equally to this work.

[*] Author for correspondence: Jun Guo, Northwest A&F University, E-mail: guojunwgq@nwafu.edu.cn; Tel: 0081-29-87082439.

Running title: Functional characterization of *PsCaMKL1* in *Pst*

This article has been accepted for publication and undergone full peer review but has not been through the copyediting, typesetting, pagination and proofreading process which may lead to differences between this version and the Version of Record. Please cite this article as an 'Accepted Article', doi: 10.1111/1462-2920.13881

Summary

Calcium/calmodulin-dependent kinases (CaMKs) are Ser/Thr protein kinases (PKs) that respond to changes in cytosolic free Ca^{2+} and play diverse roles in eukaryotes. In fungi, CAMKs are generally classified into four families CAMK1, CAMKL, RAD53, and CAMK-Unique. Among these, CAMKL constitutes the largest family. In some fungal plant pathogens members of the CaMKL family have been shown to be responsible for pathogenesis. However, little is known about their role(s) in rust fungi. In this study, we functionally characterized a novel PK gene, *PsCaMKL1*, from *Puccinia striiformis* f. sp. *tritici* (*Pst*). *Ps*CaMKL1 belongs to a group of PKs that is evolutionarily specific to basidiomyceteous fungi. *Ps*CaMKL1 shows little intra-species polymorphism between *Pst* isolates. *PsCaMKL1* transcripts are highly elevated at early infection stages, whereas gene expression is down-regulated in barely germinated urediospores under KN93 treatment. Overexpression of *PsCaMKL1* in fission yeast increased resistance to environmental stresses. Knock down of *PsCaMKL1* using host-induced gene silencing (HIGS) reduced the virulence of *Pst* accompanied by reactive oxygen species (ROS) accumulation and a hypersensitive response. These results suggest that *Ps*CaMKL1 is a novel pathogenicity factor that exerts it virulence function by regulating ROS production in wheat.

Introduction

In eukaryotic cells, protein kinases (PKs) are central components which - through reversible phosphorylation - are involved in signal transduction from environmental stimuli into the cell or between subcellular components within the cell. They affect around 30% of all protein functions including gene expression, metabolism, movement, circadian rhythm and many other processes (Hanks, 2003). The model plant *Arabidopsis thaliana* has at least 1,000 PK genes (Champion et al., 2004), while in *Homo sapiens* 518 PK genes were identified (Manning et al., 2002). Traditionally, the fungal kingdom is assigned to four phyla, including the basal fungi (Chytridiomycota, and Zygomycota), and the more recently derived monophyletic lineage, the dikarya (Ascomycota, and Basidiomycota). In the model fungus *Saccharomyces cerevisiae* 132 PK genes were identified comprising 2% of the whole genome (http://www.kinase.com/web/current/kinbase/browser/SpeciesID/4932). As for plant pathogenic fungi, there is an estimate of 116 predicted PKs for *Fusarium graminearum*, among a total of 13,321 genes (Wang et al., 2011).

Conventional PKs (ePKs) together with atypical protein kinases (aPKs) constitute the eukaryotic PK superfamily. ePKs are generally classified into nine functional groups one of which comprises the calcium/calmodulin-dependent kinases (CaMKs) (Hanks, 2003). CaMKs are Ser/Thr PKs with a highly conserved amino-terminal catalytic domain and a carboxyl-terminal regulatory domain consisting of overlapping auto-inhibitory and Ca^{2+}/CaM binding domains (Swulius and Waxham, 2008; Tamuli et al., 2011). Based on the Kinase Database kinbase

(http://www.kinase.com/web/current/kinbase/) (Goldberg et al., 2013), CAMKs in fungi can be classified into the four families CAMK1, CAMKL, RAD53, and CAMK-Unique. CAMKL forms the largest family including twelve PKs in *S. cerevisiae* and ten in *Coprinopsis cinerea*. Further classification indicates seven subfamilies Kin4, Kin1, GIN4, PASK, AMPK, CHK1, and MARK.

The diverse roles of CaMKLs are gradually being unraveled. In *S. cerevisiae*, GIN4, KCC4, and HSL1 from the GIN4 subfamily were found to regulate entry into mitosis through phosphorylation of SWE1 (Barral et al., 1999). The AMPK subfamily member Snf1 triggers transcriptional responses to glucose limitation by inhibiting the carbon catabolite repressor Mig1 and stimulating a set of transcriptional activators (Zaman et al., 2008). In the plant pathogens *Cochliobolus carbonum*, *F. oxysporum*, *M. oryzae*, or *F. graminearum* deletion of *Snf1* causes reduced expression of cell wall degrading enzyme (CWDE) genes, poor growth on non-fermentable or complex carbon sources, and a decrease in host plant colonization and disease symptoms (Tonukari et al., 2000; Ospina-Giraldo et al., 2003; Yi et al., 2008; Lee et al., 2009). However, *Snf1* is dispensable for virulence in *Ustilago maydis* (Nadal et al., 2010). Kin1 and Kin2 from the Kin1 subfamily are a pair of closely related serine/threonine PKs, regulating exocytosis through phosphorylation of the t-SNARE Sec9 (Elbert et al., 2005). Further studies revealed that Kin2 is localized to polarity sites and plays a role in septin organization (Yuan et al., 2016). *Fg*Kin1 in *F. graminearum* plays important roles in pathogenesis and growth (Luo et al., 2014). The Kin4 subfamily member KIN4, is a key regulator of the spindle position checkpoint for cells exiting

mitosis (Caydasi et al., 2010). In *A. nidulans*, the Kin4-related kinase KfsA is responsible for modulating septum formation (Takeshita et al., 2007). In *F. graminearum*, *Fg*Kin4 plays crucial roles in septum formation, conidiation and sexual reproduction (Wang et al., 2011). In the human pathogen *Cryptococcus neoformans*, functional analysis of its kinome indicated 63 kinases to be involved in pathogenicity (Lee et al., 2016).

Wheat stripe rust, caused by *Puccinia striiformis* f. sp. *tritici* (*Pst*), a biothrophic fungus, has become the largest biotic limitation to wheat production and threatens global food supply for the past 15 years. Currently, 88% of the world's wheat production is susceptible to wheat stripe rust, causing global losses of over 5 million tons with an estimated market value of $1 billion USD annually (Beddow et al., 2015). The major phase of the stripe rust life cycle is the urediospore phase. Urediospores can germinate in water, but germ tubes will die without the presence of host cells. After successful adhesion to wheat leaves, urediospores produce germ tubes, which elongate along leaf veins until they encounter stomatal openings. Settled in the substomatal chamber the fungus differentiates a substomatal vesicle (SV), infection hyphae (IHe), haustorial mother cells (HMCs), penetrates a contacted cell wall and finally forms a nutrient-absorbing structure, the haustorium (H) without breaking the plasma membrane of the host cell. Intercellular hyphae can grow as a mycelial network within the mesophyll. Then, sporogenic tissue is formed and produces the uredium close to the leaf surface, completing the asexual life cycle (Kang et al., 2002; Voegele et al., 2001; Wang et al., 2007).

A few studies have reported that PKs play important roles during initial infection, in virulence, or during biotrophic growth of rust fungi (Hu et al., 2007; Zhang et al., 2012; Panwar et al., 2013a, b; Cheng et al., 2015). However, little is known about the importance of CaMKLs in rust fungi. In this study, we characterize a novel protein kinase gene from *Pst*, designated *PsCaMKL1*, which is specific to basidiomycetes. Transcript profiles of *PsCaMKL1* during the *Pst*-wheat interaction were analyzed and the subcellular localization of *PsCaMKL1* was determined. Overexpression and knockdown of *PsCaMKL1* were performed to identify its functions in the wheat-*Pst* interaction. Our results indicate that *PsCaMKL1* is a novel pathogenicity factor that is responsible for *Pst* virulence in wheat.

Results

*Ps*CaMKL1 is a basidiomycete-specific protein kinase

To identify novel pathogenicity factors in *Pst*, we performed a detailed RNA-based sequencing approach (RNA-seq) using the susceptible wheat cultivar Yangmai158 - lacking *Yr26* (Wang et al., 2008), and the prevalent virulent *Pst* race CYR32 (Wan et al., 2004). One transcript that encodes a putative fungal PK was identified in the resulting RNAseq data. Mapping to the CYR32 genome (Zheng et al., 2013) showed it encodes a putative CaMK from the CAMK functional group (Goldberg et al., 2013). Sequence alignments using data from *Pst* isolates CYR32, and PST78 showed that there is only one copy in the *Pst* genome. The gene has an open reading frame of 1,620 bp, encoding a 540 amino acid protein with a predicted molecular mass of 59.4

kDa containing an N-terminal S_TKc domain (**Fig. S1**) and a putative 19 aa CaM-binding site (**Fig. S2**). BLASTP alignments identified Kin4 from *S. cerevisiae* (E value = 5e-22) and Ppk9 from *S. pombe* (E value = 5e-22) as closest homologs. Considering that Kin4 and Ppk9 belong to the CaMKL family in the CAMK functional group, we designated the new gene *PsCaMKL1*, for *P. striiformis* CaMK-like gene 1 (GenBank accession number KF989486.1).

Further sequence alignment showed that *Ps*CaMKL1 shares low sequence identity with Kin4 (25%) and Ppk9 (26%) and homology was largely limited to the N-terminal S_TKc domain (**Fig. S3**). Remarkably, reciprocal BLASTP searches on the *Pst* genome databases indicated that Kin4 from *S. cerevisiae* and Ppk9 from *S. pombe* are not orthologous to this putative CaMK. To further identify orthologous genes of *PsCaMKL1* in eukaryotes, we performed OrthoMCL analysis (Li et al., 2003) on genome databases of 47 species including Chromista, Fungi, Metazoa and Viridiplantae (**Table S1**). Our results indicate that one-to-one orthologous relationships only exist between *PsCaMKL1* and 17 species from the Basidiomycota only (**Table S1**). Thus, our results suggest that *PsCaMKL1* is a novel PK gene that is unique to Basidiomycota. Further sequence analysis of *Ps*CaMKL1 and its orthologs revealed that they all possess a S_TKc or Pkinase domain (**Fig. S1**) and a 19-22 aa CaM-binding site (**Fig. S2**). Notably, orthologs of CaMKL1 proteins in the three rust fungi of the genus *Puccinia* (*Pst*, *P. triticina,* and *P. graminis* f. sp. *tritici*) seem to be very similar to each other, with up to 70% and 76% sequence identity, respectively. Phylogenetic analysis of *Ps*CaMKL1 and its orthologs indicated that *Ps*CaMKL1 has

a much closer relationship with its orthologs from Pucciniomycotina than those from Ustilaginomycotina and Agaricomycotina (**Fig. 1**).

PsCaMKL1 is highly conserved between *Pst* isolates

To identify intra-species polymorphisms in *PsCaMKL1*, we compared the coding regions of seven sequenced *Pst* isolates, including a Chinese isolate (CYR32), four US isolates (PST21, PST43, PST78, and PST130) and two UK isolates (PST-08/21, and PST87-7). Compared with *PsCaMKL1* from CYR32, only one synonymous substitution was observed among all seven *Pst* isolates (**Table S2**). Thus, *PsCaMKL1* seems highly conserved between *Pst* isolates suggesting an essential function.

PsCaMKL1 is highly induced at early infection stages of *Pst*

To analyze *PsCaMKL1* transcript profiles during different *Pst* differentiation stages, we assayed transcript abundance by quantitative real-time PCR (qRT-PCR). qRT-PCR assays indicated that *PsCaMKL1* is highly induced at early stages of *Pst* infection (6, 12, 18, and 24 hours post inoculation (hpi)), and culminated at 20.7-fold at 6 hpi (**Fig. 2**). During secondary hyphae formation (48, 72, 120, and 168 hpi), transcript levels were again similar to that of the urediospore stage (**Fig. 2**). Thus, *PsCaMKL1* transcript levels seem to be elevated during early infection stages.

PsCaMKL1 transcripts are down-regulated in barely germinated urediospores

To determine whether *Ps*CaMKL1 is involved in urediospore germination of *Pst*, we tested the effects of the CaMK selective inhibitor KN93 (Sumi et al. 1991) on germination. *Pst* urediospores were incubated with water (control; **Fig. 3A**), or

different concentrations of KN93 (**Fig. 3B**). The germination rate of urediospores was significantly decreased as the KN93 concentration was increased to 0.8 μM. At 1.4 μM only 8.02% germination was observed (**Fig. 3C**).

To analyze transcript levels of *PsCaMKL1* after KN93 treatment (1.4 μM) (barely germinated urediospores), we performed qRT-PCR with *PsEF1* and *PsACT1* as controls. *PsACT1* has been revealed that it is closely related to the tip growth of urediospores of *Pst* (Liu et al. 2012). The transcript levels of *PsCaMKL1* and *PsACT1* significantly decreased to 3.08% and 3.64% at 6 hours post treatment (hpt), respectively. In contrast, *PsEF1* transcripts showed no significant change (**Fig. 3D**). Our results indicate that KN93 significantly affects *Pst* urediospore germination, and that transcription of *PsCaMKL1* seems suppressed in barely germinated urediospores.

Overexpression of *PsCaMKL1* in fission yeast increases its resistance to environmental stresses

Ca^{2+}/CaMKs in *N. crassa* have been found to regulate multiple cellular functions such as growth, thermotolerance and oxidative stress tolerance (Kumar and Tamuli, 2014). To investigate the role of *PsCaMKL1* in response to stresses, we performed a *PsCaMKL1*-overexpression assay in *S. pombe* using the vector pREP3X (Forsburg, 1993). *PsSRPKL* was chosen as positive control, since it was reported to affect yeast cell morphology and the responses to environmental stimuli (Cheng et al., 2015). Empty pREP3X vector and GFP-carrying pREP3X were chosen as negative controls. Yeast cells were cultured in inducing (-Thiamine), or repressing (+Thiamine) medium for 20 h. Cell morphology of pREP3X-*PsCaMKL1,* pREP3X-*GFP* and pREP3X

transformants cultured in inducing or repressing medium appeared to be normal (**Fig. 4A**). However, pREP3X-*PsSRPKL* in inducing medium showed a significant shorter length of the cell major axis (**Fig. 4A, B**). Therefore, overexpression of *PsCaMKL1* seems to have no effect on cell morphology. Under H_2O_2 (**Fig. 4C**) and NaCl (**Fig. 4D**) challenge, the number of colony forming units of pREP3X-*PsCaMKL1* transformants was much higher in inducing than that in repressing medium compared to pREP3X-*GFP* and pREP3X transformants ($P < 0.01$). In contrast, overexpression of *PsSRPKL* induced aberrant morphology and decreases resistance to environmental stimuli (**Fig. 4**). These results demonstrate that overexpression of *PsCaMKL1* in fission yeast increases resistance to environmental stresses.

Knockdown of *PsCaMKL1* reduces virulence of *Pst* on wheat

To determine whether *Ps*CaMKL1 is involved in *Pst* pathogenicity, we silenced *PsCaMKL1* using the BSMV-HIGS system. All BSMV-inoculated plants exhibited mild chlorotic mosaic symptoms at 10 days post inoculation (dpi) (**Fig. 5A**). However, no obvious defects were observed during subsequent growth. In BSMV:TaPDS plants, a bleaching phenotype was observed at 14 dpi (**Fig. 5A**), indicating that the BSMV-HIGS system is functional. The fourth leaves of wheat plants were inoculated with CYR32, and rust phenotypes were photographed at 14 dpi. Wheat leaves inoculated with BSMV:PsCaMKL1-as1, or BSMV:PsCaMKL1-as2 showed greatly increased resistance with fewer uredia (**Fig. 5B**), and smaller clefts (**Fig. 5C**).

To determine silencing efficiency, transcript levels of *PsCaMKL1* were assayed at 24, 48 and 120 hpi by qRT-PCR. Compared with transcript levels of *PsCaMKL1* in

leaves inoculated with BSMV:γ, *PsCaMKL1* levels in leaves inoculated with BSMV: PsCaMKL1-as1 were reduced by 73%，60%, and 46% at 24, 48 and 120 hpi, respectively (**Fig. 5D**). Similarly, in plants carrying the BSMV:PsCaMKL1-as2 construct, transcript levels of *PsCaMKL1* were reduced by 73%, 55%, and 44% at 24, 48 and 120 hpi, respectively (**Fig. 5D**). In addition, pustule density and average area of the cleft on *PsCaMKL1*-silenced leaves were calculated. Pustule density on leaves inoculated with BSMV:PsCaMKL1-as1, or BSMV:PsCaMKL1-as2 was decreased by 43.7% and 31.6%, respectively (**Fig. 5E**). Through SEM observation, the area of the clefts on wheat leaves inoculated with BSMV:PsCaMKL1-as1, or BSMV:PsCaMKL1-as2 was reduced to 34.1% and 36.2% of the control, respectively (**Fig. 5F**). These results indicate that *Ps*CaMKL1 contributes significantly to *Pst* virulence on wheat.

HIGS of *PsCaMKL1* impedes fungal growth and increases H_2O_2 accumulation in wheat cells

To determine whether there is a difference in hyphal growth and infection structure formation between BSMV:PsCaMKL1 treated and control plants (BSMV:γ), we assayed histological changes in HIGS-silenced plants inoculated with *Pst* **(Fig. S4)**. No significant difference in number of hyphal branches and haustorial mother cells were found between *PsCaMKL1*-silenced and control plants at 24 hpi (**Table S3**). Hyphal length of control plants and MOCK (non-treated) plants showed no significant difference (**Fig. 6A**). However, hyphal length in BSMV:PsCaMKL1-as1, or BSMV:PsCaMKL1-as2 treated plants was significantly shorter at 24, 48 and 120 hpi

(**Fig. 6A**).

To determine whether transcript levels of defense-related genes in *PsCaMKL1*-silenced wheat plants are affected, we assayed *TaPR1* at 24, 48, and 120 hpi. Knocking down *PsCaMKL1* significantly increased transcript levels of *TaPR1* on wheat leaves inoculated with BSMV:PsCaMKL1-as1, or BSMV:PsCaMKL1-as2 at 24 hpi ($P < 0.05$) (**Fig. 6B**).

To analyze the host response, H_2O_2 accumulation, the ratio of necrotic wheat cells and transcript profiles of *TaCAT,* whose product is involved in ROS-scavenging, were analyzed. ROS response occurred in *PsCaMKL1*-knockdown plants at 24, 48, and 120 hpi (**Fig. 7A-I**), and cell death appeared at 120 hpi (**Fig. 7J-L**). Higher levels of ROS production in *PsCaMKL1*-knockdown plants were observed at 24 (**Fig. 7M**), 48 (**Fig. 7N**) and 120 hpi (**Fig. 7O**). Similarly, the number of necrotic cells per infection site in *PsCaMKL1*-knockdown plants was much higher than in control plants at 120 hpi (**Fig. 7P**). In addition, transcript levels of *TaCAT* (**Fig. 7Q**) were significantly increased at 24 hpi in *PsCaMKL1*-knockdown plants. These results indicate that *PsCaMKL1* is likely involved in responses to oxidative stress in *Pst* and in overcoming plant defense responses.

Discussion

Systematic functional analyses of the fungal kinome identified some unique kinases in human pathogenic fungus *C. neoformans* (Lee et al., 2016), as well as in the phytopathogenic fungus *F. graminearum* (Wang et al., 2011). In this study, we

identified a novel basidomycete-specific *PsCaMKL1*, which is highly induced at early stages of *Pst* infection and functions as a pathogenicity factor.

PsCaMKL1 transcript levels are up-regulated during urediospore germination, and expression is down regulated when the germination of urediospores is blocked by the inhibitor KN93. Urediospore germination is the beginning of asexual infection in rust fungi, consisting of several morphological and biological alterations, such as spore swelling, adhesion, nuclear migration and rearrangement of the microfibrillar network (Wang and McCallum, 2009). Our results suggest that *PsCaMKL1* may participate in the complex signaling pathway or metabolism activity during germ tube formation. *PsCaMKL1* transcripts showed a 5~10 fold increase at early infection stages (12-24 hpi). This time frame comprises the differentiation of the substomatal vesicle, the formation of the haustorial mother cell, and the formation of the first haustorium (Wang et al., 2007). Silencing of *PsCaMKL1* via HIGS significantly reduced hyphal length and sporulation. Protein kinases have been implicated in the regulation of many processes that guide pathogen development throughout the course of infection (Turra et al., 2014). Therefore, *PsCaMKL1* maybe act as a pathogenicity factor through its involvement in growth and development of *Pst*.

The ability to survive stress and environmental stimuli provides a clear advantage for a pathogen (Hamel et al., 2012; Turra et al., 2014). In this study, knockdown of *PsCaMKL1* decreased *Pst* resistance to oxidative stress. This decrease together with a lower suppression of host plant defense reactions may explain the increased host production of ROS (H_2O_2) and the following cell necrosis. Consistently,

overexpression of *PsCaMKL1* in fission yeast increased resistance to oxidative and hyperosmotic stresses. Our data suggest that *Ps*CaMKL1 plays an important role in *Pst* adaptation to environment stimuli. However, further studies are needed to uncover the mechanism how *Ps*CaMKL1 regulates multiple cellular functions in *Pst* in response to diverse stresses.

Although PKs show conserved characters across all eukaryotes, this group of kinases is plastic and prone to expansion (Goldberg et al., 2013). Sequence analysis revealed that *Ps*CaMKL1 and its orthologs are conserved in the N-terminal S_TKc or Pkinase domain (**Fig. S1**). However, *Ps*CaMKL1 and its orthologs from Pucciniomycotina, Agricomycotina, and Ustilaginomycotina exhibit a higher degree of variability in the C-terminal region. These results suggest that these novel CaMKLs in Basidiomycota may have diverse functions under stresses. In our study the *Ps*CaMKL1 ortholog from *C. neoformans* (XP_02053401.1) was classified into CAMK/CAMKL, while Lee et al. (2016) classified it into the PDHK group by Kinomer 1.0 (Martin et al., 2009) analysis. The reason may be the difference of the two classification databases and/or the uniqueness of *Ps*CaMKL1 and its orthologs in the Basidiomycota. However, *Ps*CaMKL1 is classified into the CAMK/CAMKL via both databases (KinBase and Kinomer 1.0).

Kinases are considered the second largest protein class for drug targeting (Rask-Andersen et al., 2014). In both *Dictyostelium discoideum* and *Giardia lamblia*, specific kinases have been identified that are hypothesized to be required for habitat- or lifestyle-specific processes. These kinases are logical targets for biologic-

and/or pharmaceutical-based antimicrobials (Goldberg et al., 2006; Manning et al., 2011). This highlights their importance also in the view of identifying novel fungicides. In *F. graminearum*, three out of 24 *PK* genes that have no distinct orthologs in yeast seem to be important for plant infection (Wang et al., 2011). In *C. neoformans*, virulence-related kinase (Vrk1) and infectivity-related kinase 1-7 (Irk1-7) are included in a group of 63 pathogenicity-related kinases which show no orthologs in model yeasts (Lee et al., 2016). The fact that *Ps*CaMKL1 must be regarded as a pathogenicity factor for *Pst* and the uniqueness of this group of PKs among the Basidiomycota, makes them ideal targets for the development of control agents which will not harm the microbial population, or host and non-host plants. Human health, food security and safety, and the environment will also not be affected.

PsCaMKL1 seems to be a specific pathogenicity factor in rust fungi, which contributes to urediospore germination, plant infection and virulence probably by phosphorylating its substrates to regulate fungal growth and respond to plant defenses. Therefore, identification and characterization of other basidiomycete-specific, especially rust fungi-specific, PKs and their targets in the future will result in a better understanding of pathogenesis and virulence evolution in *Pst* and other basidiomycetes.

Experimental procedures

Plant materials, strains and culture conditions

Wheat cultivar Suwon 11 (Su11) was grown in a controlled environment chamber

at 20°C with 60% relative humidity and a 16 h / 8 h day/night photoperiod. Chinese *Pst* race CYR32 was inoculated and propagated on wheat cv. Su11 as described (Ma et al., 2009). *Escherichia coli* JM109 cultures were grown in Luria-Bertani (LB) medium or on LB-agar plates with antibiotics of appropriate concentrations at 37°C for plasmid constructions.

Isolation and sequence analysis of *PsCaMKL1*

The conserved domains of *Ps*CaMKL1 and other proteins were deduced using NCBI conserved domain searches (http://www.ncbi.nlm.nih.gov/Structure/cdd/wrpsb.cgi). Calmodulin binding sites were identified using the Calmodulin Target Database (Yap et al., 2000). Multiple sequence alignments were performed with ClustalW2.0 (Chenna et al., 2003) and DNAMAN7.0 software (Lynnon Biosoft, San Ramon, CA, USA). Phylogenetic trees were constructed using the software MEGA7.0 (Kumar et al., 2016).

RNA extraction and cDNA synthesis

To analyze transcript levels, samples of urediospores, and infected wheat leaves at 6, 12, 18, 24, 48, 72, 120, 168 hpi were collected. To calculate HIGS efficiency, the fourth wheat leaves inoculated with CYR32 at 24, 48, 120 hpi were harvested. To analyze transcript levels of *PsCaMKL1, PsEF1* and *PsACT1* after treatment with inhibitor KN93, samples were taken at 6 hpt. Total RNA was extracted using TRIzol™ Reagent (Invitrogen, Carlsbad, CA, USA) according to the manufacturer's instructions. First-strand cDNA was synthesized from 2 μg total RNA of each sample using the SMART™ reverse transcription Kit (Clontech Laboratories Inc., Mountain

View, CA, USA) following the manufacturer's directions.

Quantitative RT-PCR

Primers used in this study are listed in **Table S4**. Quantitative RT-PCR (qRT-PCR) assays were performed using a CFX Connect Real-Time System (Bio-Rad, Hercules, CA, USA). Amplification was performed as follows: 95°C for 1 min, followed by 40 cycles of 10 s at 95°C, 20 s at 60°C and 40 s at 72°C. Transcript levels of genes were calculated by the $2^{-\Delta\Delta C}{}_{T}$ method (Livak and Schmittgen, 2001) with *PsEF1* and *TaEF1α* as endogenous reference, respectively, for normalization as previously described (Guo et al., 2011). Transcript abundance was assessed with three independent biological replicates.

Vector construction

For HIGS experiments, plasmid construction followed a previously described protocol (Yin et al., 2011). Two fragments of *PsCaMKL1* were amplified with *Not*I and *Pac*I restriction sites using two pairs of specific primers (**Table S4**). Products were then ligated to the digested BSMV:γ vector. For over-expression in fission yeast, the vector pREP3X (Forsburg, 1993) was used. A double digest with restriction enzymes *Sal*I and *Bam*HI of PCR products obtained with primers PsCaMKL1-prep-F and PsCaMKL1-prep-R (**Table S4**) was performed and the fragment ligated into pREP3X. Negative control pREP3X-GFP and positive control pREP3X-PsSRPKL were generated from previous study (Cheng et al., 2015). All plasmids were confirmed by sequencing.

Overexpression of *PsCaMKL1* in fission yeast

pREP3X-*PsCAMKL1*, pREP3X, pREP3X-*PsSRPKL*, and pREP3X-*GFP* were transformed into *S. pombe* by electroporation. Thiamine was used as repressor for the nmt1-promoter. Verified transformed cells were incubated in medium with or without thiamine with a starting density of OD_{600}=0.2 for 20 h. Cell growth assay on yeast solid media plates containing 2 mM H_2O_2 or 0.35 M NaCl were performed with 100 µL OD_{600}=0.1 from logarithmic cultures.

HIGS assay

Two fragments of *PsCaMKL1* were selected for HIGS assay (**Fig. S5**). Capped *in vitro* transcripts were prepared from linearized plasmid γ-PDS-as, γ- *PsCaMKL1*-1as, γ-*PsCaMKL1*-2as, γ, α, β using the Message T7 *in vitro* transcription kit (Ambion, Austin, TX, USA) following the manufacturer's directions. BSMV:γ-PDS, wheat PDS gene acted as the positive control. BSMV:γ as was used as negative control. A 1:1:1 mixture of the three components of the viral genome (α, β, and γ, γ-derived constructs) from *in vitro* transcription reactions was mixed with 45 µl of FES buffer. The mixture was applied to the second fully expended leaf of around 13 day old wheat plants by rubbing inoculation (Scofield et al., 2005). Seedlings were kept in controlled environmental chambers at 25 ± 2°C with 16 h of light and 8 h darkness. Ten days later, when viral symptoms appeared, the fourth leaves were inoculated with urediospores of *Pst* isolate CYR32. Samples of the inoculated leaves for qRT-PCR and histological observation were taken at 24, 48 and 120 hpi. Rust infection phenotypes were recorded, photographed and sampled for cytological observation at

14 dpi.

Histological observation of *Pst* growth in wheat leaves

Wheat leaves were fixed and decolorized in ethanol/tri-chloromethane (3/1; v/v) with 0.15% (w/v) tri-chloroacetic acid for 3 days and then cleared in saturated chloral hydrate as described previously (Wang et al., 2007). To visualize pathogen structures, samples were stained with wheat germ agglutinin (WGA) conjugated to Alexa 488 (Invitrogen, USA) (Ayliffe et al., 2011). H_2O_2 production was detected in plant tissue by staining with 3-3' diaminobenzidine (DAB) (Amresco, Solon, OH, USA). Specimen preparations and microscopic observations were performed following procedures previously described (Wang et al., 2007). Autofluorescence of mesophyll cells was observed with an epifluorescence microscope (excitation filter, 485 nm; dichromic mirror, 510 nm; and barrier filter, 520 nm).

All microscopic examinations were done with an Olympus BX-53 microscope (Olympus Corporation, Tokio, Japan). For each sample, at least 50 infection units from at least eight leaf segments were examined and the data were analyzed by SPSS version 16.0 (SPSS, Chicago, IL, USA). Data are presented as mean ± SE.

Scanning electron microscopy

To observe the ultrastructure of pustules, leaves samples were cut into 0.5*0.5 cm pieces, fixed in 4% glutaraldehyde (0.2 M phosphate buffer, pH=6.8) at 4^oC overnight. Then, leaves were washed with phosphate buffer four times, each for 15 min. Thereafter, gradually dehydration was done by ethanol from 30, 50, 70, 80 to 90%, each for 15 min and finally 100% ethanol for three times, each for 30 min. At last,

samples were treated with isoamyl acetate twice, each for 20 min. The samples were sputter-coated with gold in an E-1045 (Hitachi, Japan) after drying in a CO_2 vacuum, and finally were examined with an S-4800 SEM (Hitachi Ltd., Tokio, Japan).

Acknowledgements

This study was financially supported by the National Basic Research Program of China (No. 2013CB127700), the National Natural Science Foundation of China (No. 31371889 and 31171795), and the 111 Project from the Ministry of Education of China (No. B07049).

Figure legends

Fig. 1. Phylogeny of *Ps*CaMKL1 and its orthologs. The phylogenetic tree was constructed with the Maximum-likelihood (ML) method using MEGA 7.0 software with 1,000 bootstrap values. CaMK1 from *Homo sapiens* is used as out-group. Branches are labeled with GenBank accession numbers and protein names. For abbreviations, see supporting information Table S1.

Fig. 2. Transcript profiles of *PsCaMKL1* at different *Pst* infection stages. Transcript levels of *PsCaMKL1* were calculated by the $2^{-\Delta\Delta C}{}_{T}$ method with the elongation factor gene of *Pst* as endogenous reference. Values represent mean ± standard errors of three independent replicates. Differences were calculated by Student's t-tests. Asterisks indicate $P < 0.05$, double asterisks indicate $P < 0.01$. U, urediospores.

Fig. 3. Transcript levels of *PsCaMKL1* were significantly decreased in barely germinated urediospores. (A) Germinated urediospores after 10 h treated with water (control). (B) Urediospores after 10 h treated with KN93 (1.4 μM). (C) The germination rate of *Pst* urediospores decreased gradually as KN93 concentration increased. (D) Transcript levels of *PsCaMKL1* were significantly decreased in barely germinated urediospores at 6 hours post treatment with KN93 (1.4 μM). Values represent means ± standard errors of three independent replicates. Differences were calculated by Student's t-tests. Asterisks indicate $P < 0.05$ and double asterisks indicate $P < 0.01$.

Fig. 4. Effects of overexpression of *PsCaMKL1* in fission yeast. No significant morphological changes (A) and length change (B) were observed in *PsCaMKL1*-overexpressing yeast. Bars = 10 μm. The average number of growing yeast colonies under oxidative stress (C) and hyperosmotic stress (D) under inducing, or repressing conditions were calculated. Values represent means ± standard errors of three independent replicates. Differences were calculated by Student's t-tests. Double asterisks indicate $P < 0.01$.

Fig. 5. Functional characterization of *PsCaMKL1* using the BSMV-HIGS system**.** (A) Fourth leaves of plants with mild mosaic symptoms inoculated with buffer (mock), BSMV:PDS, BSMV:γ (vector control), BSMV:PsCaMKL1-as1, or BSMV:PsCaMKL1-as2 at 10 dpi. BSMV:TaPDS exhibits the expected photo-bleaching phenotype. (B) Phenotypes of the fourth leaves inoculated with buffer (mock), BSMV:γ (empty vector), PsCaMKL1-as1, or BSMV:PsCaMKL1-as2 14 dpi with the virulent *Pst* isolate CYR32. (C) Observation of the clefts on the fourth leaves of wheat plants inoculated with BSMV:γ, BSMV:PsCaMKL1-as1, or BSMV:PsCaMKL1-as2 at 14 dpi with the virulent *Pst* isolate CYR32 under the scanning electron microscope. Bars = 500 μm. (D) Relative transcript abundance of *PsCaMKL1* in knock-down wheat leaves. RNA samples were isolated from the fourth leaves of wheat infected with BSMV:γ, BSMV:PsCaMKL1-as1, or BSMV:PsCaMKL1-as2 at 24, 48 and 168 hpi with the CYR32 isolate. Values are

expressed relative to an endogenous *Pst* reference gene *EF1*, with the empty vector (BSMV:γ) set at 1. (E) Quantification of the density of *Pst* urediospores in silenced plants 14 dpi with the CYR32 isolate. (F) Quantification of the relative average area of the cleft in silenced plants 14 dpi with the CYR32 isolate. Values represent means ± standard errors of three independent samples. Differences were assessed using Student's t-tests. Asterisks indicate $P < 0.05$ and double asterisks indicate $P < 0.01$.

Fig. 6. HIGS of *PsCaMKL1* shows compromised fungal development in wheat cells. HIGS of *PsCaMKL1* showed significantly decreased hyphal length at 24, 48 and 120 hpi. (A) Hyphal length was the average distance of the longest hypha from the origin on the substomatal vesicle (SV) to the hyphal apex; measurement was done on DP-BSW software. (B) Transcript levels of *TaPR1* (GenBank: KR351308.1) in *PsCaMKL1*-knockdown compared to control plants. Values represent means ± standard errors of three independent samples. Differences were assessed using Student's t-tests. Asterisks indicate $P < 0.05$.

Fig. 7. Production of H_2O_2 and hypersensitive cell death in control and *PsCaMKL1*-silenced plants challenged with CYR32. H_2O_2 production was observed by DAB staining. Cell death was detected as autofluorescence. (A-I) Histological observation of the host response in wheat infected with BSMV:γ, or recombinant BSMV after inoculation with CYR32. H_2O_2 accumulation at 24 hpi (A-C), 48 hpi (D-F), and 120 hpi (G-I) in BSMV:γ, BSMV:PsCaMKL1-as1, or

BSMV:PsCaMKL1-as2 infected plants. (J-L) Hypersensitive cell death at 120 hpi in BSMV:γ, BSMV:PsCaMKL1-as1, or BSMV:PsCaMKL1-as2 infected plants. (M-P) Level of ROS production and infection site with necrotic cells in wheat infected by BSMV:γ, or recombinant BSMV after inoculation with CYR32. Level of ROS production at 24 hpi (M), 48 hpi (N) and 120 hpi (O) in BSMV:γ, BSMV:PsCaMKL1-as1, or BSMV:PsCaMKL1-as2 infected plants. Number of infection sites with necrotic cells at 120 hpi (P) in BSMV:γ, BSMV:PsCaMKL1-as1, or BSMV:PsCaMKL1-as2 infected plants. White arrowheads show the position of H_2O_2 accumulation. Black arrowheads show the position of necrotic cells. Bars = 20 μm. (Q) Transcript levels of *TaCAT* (GenBank: X94352.1) in *PsCaMKL1*-knockdown compared to control plants. Values represent means ± standard errors of three independent replicates. Differences were calculated by Student's t-tests. Asterisks indicate $P < 0.05$ and double asterisks indicate $P < 0.01$.

Supporting Information

Fig. S1. Conserved domain assay of *Ps*CaMKL1 and its orthologs in Basidiomycota by CD-search (http://www.ncbi.nlm.nih.gov/Structure/cdd/wrpsb.cgi).

Fig. S2. Calmodulin binding site prediction in *Ps*CaMKL1 and its orthologs by the Calmodulin Target Database (http://calcium.uhnres.utoronto.ca/ctdb/ctdb/sequence.html).

Fig. S3. Sequence alignment of *Ps*CaMKL1 and the closest homologs *Sc*Kin4 and *Sp*Ppk9. The conserved S_TKc domains are indicated.

Fig. S4. Histological observation of fungal development. Leaves inoculated with CYR32 were sampled at 24, 48, and 120 hpi and examined under an epifluorescence microscope. A, B, and C are BSMV:γ, BSMV:PsCaMKL1-as1, and BSMV:PsCaMKL1-as2 treatments at 24 hpi. D, E, and F are the same treatments at 48 hpi. G, H, and I are treatments at 120 hpi. Bars = 20 μm. SV, substomatal vesicle; IH, infection hypha; HMC, haustorial mother cell; H, haustorium.

Fig. S5. The two fragments used to silence *PsCaMKL1*.

Table S1. The closest homologs (paralogs and orthologs) of *Ps*CaMKL1 obtained from 46 species by OrthoMCL analysis.

Table S2. Single nucleotide polymorphisms (SNPs) assay of *PsCaMKL1* among different isolates of *Pst* from different countries.

Table S3. Histological observation of fungal development at 24 hpi in wheat.

Table S4. Primers used in this study.

References

Ayliffe, M., Devilla, R., Mago, R., White, R., Talbot, M., Pryor, A., and Leung, H. (2011) Nonhost resistance of rice to rust pathogens. *Mol Plant Microbe Interact* **24**: 1143-1155.

Barral, Y., Parra, M., Bidlingmaier, S., and Snyder, M. (1999) Nim1-related kinases coordinate cell cycle progression with the organization of the peripheral cytoskeleton in yeast. *Genes Dev* **13**: 176-187.

Beddow, J.M., Pardey, P.G., Chai, Y., Hurley, T.M., Kriticos, D.J., Braun, H.J., *et al*. (2015) Research investment implications of shifts in the global geography of wheat stripe rust. *Nat Plants* **1**: 15132.

Caydasi, A.K., Kurtulmus, B., Orrico, M.I.L., Hofmann, A., Ibrahim, B., and Pereira, G. (2010) Elm1 kinase activates the spindle position checkpoint kinase Kin4. *J Cell Biol* **190**: 975-989.

Champion, A., Kreis, M., Mockaitis, K., Picaud, A., and Henry, Y. (2004) Arabidopsis kinome: after the casting. *Funct Integr Genomics* **4**: 163-187.

Cheng, Y.L., Wang, X.J., Yao, J.N., Voegele, R.T., Zhang, Y.R., Wang, W.M., *et al*. (2015) Characterization of protein kinase *PsSRPKL*, a novel pathogenicity factor in the wheat stripe rust fungus. *Environ Microbiol* **17**: 2601-2617.

Chenna, R., Sugawara, H., Koike, T., Lopez, R., Gibson, T.J., Higgins, D.G., and Thompson, J.D. (2003) Multiple sequence alignment with the Clustal series of programs. *Nucleic Acids Res* **31**: 3497-3500.

Elbert, M., Rossi, G., and Brennwald, P. (2005) The yeast Par-1 homologs Kin1 and Kin2 show genetic and physical interactions with components of the exocytic machinery. *Mol Biol Cell* **16**: 532-549.

Forsburg, S.L. (1993) Comparison of *Schizosaccharomyces pombe* expression systems. *Nucleic Acids Res* **21**: 2955-2956.

Goldberg, J.M., Griggs, A.D., Smith, J.L., Haas, B.J., Wortman, J.R., and Zeng, Q.D. (2013) Kinannote, a computer program to identify and classify members of the eukaryotic protein kinase superfamily. *Bioinformatics* **29**: 2387-2394

Goldberg, J.M., Manning, G., Liu, A., Fey, P., Pilcher, K.E., Xu, Y., and Smith, J.L. (2006) The dictyostelium kinome-analysis of the protein kinases from a simple model organism. *PLoS Genet* **2**: e38.

Guo, J., Dai, X.W., Xu, J.R., Wang, Y.L., Bai, P.F., Liu, F.R. et al. (2011) Molecular characterization of a Fus3/Kss1 type MAPK from *Puccinia striiformis* f. sp *tritici*, PsMAPK1. *PLoS ONE* **6**: e21895.

Hamel, L.P., Nicole, M.C., Duplessis, S., and Ellis, B.E. (2012) Mitogen-activated protein kinase signaling in plant-interacting fungi: distinct messages from conserved messengers. *Plant Cell* **24**: 1327-1351.

Hanks, S.K. (2003) Genomic analysis of the eukaryotic protein kinase superfamily: a perspective. *Genome Biol* **4**: 111.

Hu, G., Linning, R., McCallum, B., Banks, T., Cloutier, S., Butterfield, Y., *et al*. (2007) Generation of a wheat leaf rust, *Puccinia triticina*, EST database from stage-specific cDNA libraries. *Mol Plant Pathol* **8**: 451-467.

Kang, Z.S., Huang, L.L., and Buchenauer, H. (2002) Ultrastructural changes and localization of lignin and callose in compatible and incompatible interactions between wheat and *Puccinia striiformis*. *J Plant Dis Protect* **109**: 25-37.

Kumar, R., and Tamuli, R. (2014) Calcium/calmodulin-dependent kinases are involved in growth, thermotolerance, oxidative stress survival, and fertility in *Neurospora crassa*. *Arch Microbiol* **196**: 295-305.

Kumar, S., Stecher, G., and Tamura, K. (2016) MEGA7: molecular evolutionary genetics analysis version 7.0 for bigger datasets. *Mol Biol Evol* **33**: 1870-1874.

Lee, K.T., So, Y.S., Yang, D.H., Jung, K.W., Choi, J., Lee, D.G. et al. (2016) Systematic functional analysis of kinases in the fungal pathogen *Cryptococcus neoformans*. *Nat Commun* **7**: 12766.

Lee, S.H., Lee, J., Lee, S., Park, E.H., Kim, K.W., Kim, M.D., *et al*. (2009) *GzSNF1* is required for normal sexual and asexual development in the ascomycete *Gibberella zeae*. *Eukaryot Cell* **8**: 116-127.

Li, L., Stoeckert, C.J., and Roos, D.S. (2003) OrthoMCL: Identification of ortholog groups for eukaryotic genomes. *Genome Res* **13**: 2178-2189.

Liu, J., Zhang, Q., Chang, Q., Zhuang, H., Huang, L.L., and Kang, Z.S. (2012). Cloning and characterization of the actin gene from *Puccinia striiformis* f. sp. *tritici*. *World J Microbiol Biotechnol* **28**: 2331-2339.

Livak, K.J., and Schmittgen, T.D. (2001) Analysis of relative gene expression data using real-time quantitative PCR and the $2^{-\Delta\Delta C}{}_{T}$ Method. *Methods* **25**: 402-408.

Luo, Y.P., Zhang, H.C., Qi, L.L., Zhang, S.J., Zhou, X.Y., Zhang, Y.M., and Xu, J.R. (2014) *Fg*Kin1 kinase localizes to the septal pore and plays a role in hyphal growth, ascospore germination, pathogenesis, and localization of Tub1 beta-tubulins in *Fusarium graminearum*. *New Phytol* **204**: 943-954.

Ma, J.B., Huang, X.L., Wang, X.J., Chen, X.M., Qu, Z.P., Huang, L.L., and Kang, Z.S. (2009) Identification of expressed genes during compatible interaction between stripe rust (*Puccinia striiformis*) and wheat using a cDNA library. *BMC Genomics* **10**: 586.

Manning, G., Whyte, D.B., Martinez, R., Hunter, T., and Sudarsanam, S. (2002) The protein kinase complement of the human genome. *Science* **298**: 1912-1934.

Manning, G., Reiner, D.S., Lauwaet, T., Dacre, M., Smith, A., Zhai, Y., *et al*. (2011) The minimal kinome of *Giardia lamblia* illuminates early kinase evolution and unique parasite biology. *Genome Biol* **12**: R66.

Martin, D.M., Miranda-Saavedra, D., and Barton, G.J. (2009) Kinomer v. 1.0: a database of systematically classified eukaryotic protein kinases. *Nucleic Acids Res* **37**: D244-D250.

Nadal, M., Garcia-Pedrajas, M.D., and Gold, S.E. (2010) The *snf1* gene of *Ustilago maydis* acts as a dual regulator of cell wall degrading enzymes. *Phytopathology* **100**: 1364-1372.

Ospina-Giraldo, M.D., Mullins, E., and Kang, S. (2003) Loss of function of the *Fusarium oxysporum SNF1* gene reduces virulence on cabbage and *Arabidopsis*. *Curr Genet* **44**: 49-57.

Panwar, V., McCallum, B., and Bakkeren, G. (2013a) Host-induced gene silencing of

wheat leaf rust fungus *Puccinia triticina* pathogenicity genes mediated by the Barley stripe mosaic virus. *Plant Mol Biol* **81**: 595-608.

Panwar, V., McCallum, B., and Bakkeren, G. (2013b) Endogenous silencing of *Puccinia triticina* pathogenicity genes through in planta-expressed sequences leads to the suppression of rust diseases on wheat. *Plant J* **73**: 521-532.

Rask-Andersen, M., Masuram, S., and Schioth, H.B. (2014) The druggable genome: Evaluation of drug targets in clinical trials suggests major shifts in molecular class and indication. *Annu Rev Pharmacol Toxicol* **54**: 9-26.

Scofield, S.R., Huang, L., Brandt, A.S., and Gill, B.S. (2005) Development of a virus-induced gene-silencing system for hexaploid wheat and its use in functional analysis of the *Lr21*-mediated leaf rust resistance pathway. *Plant Physiol* **138**: 2165-2173.

Sumi, M., Kiuchi, K., Ishikawa, T., Ishii, A., Hagiwara, M., Nagatsu, T., *et al*. (1991) The newly synthesized selective Ca^{2+}/calmodulin dependent protein kinase II inhibitor KN-93 reduces dopamine contents in PC12h cells. *Biochem Biophys Res Commun* **181**: 968-975.

Swulius, M.T., and Waxham, M.N. (2008) Ca^{2+}/calmodulin-dependent protein kinases. *Cell Mol Life Sci* **65**: 2637-2657.

Takeshita, N., Vienken, K., Rolbetzki, A., and Fischer, R. (2007) The *Aspergillus nidulans* putative kinase, KfsA (kinase for septation), plays a role in septation and is required for efficient asexual spore formation. *Fungal Genet Biol* **44**: 1205-1214.

Tamuli, R., Kumar, R., and Deka, R. (2011) Cellular roles of neuronal calcium sensor-1 and calcium/calmodulin-dependent kinases in fungi. *J Basic Microbiol* **51**: 120-128.

Tonukari, N.J., Scott-Craig, J.S., and Walton, J.D. (2000) The *Cochliobolus carbonum SNF1* gene is required for cell wall-degrading enzyme expression and virulence on maize. *Plant Cell* **12**: 237-247.

Turra, D., Segorbe, D., and Di Pietro, A. (2014) Protein kinases in plant-pathogenic fungi: conserved regulators of infection. *Annu Rev Phytopathol* **52**: 267-288.

Voegele, R.T., Struck, C., Hahn, M., and Mendgen, K. (2001) The role of haustoria in sugar supply during infection of broad bean by the rust fungus *Uromyces fabae*. *Proc Nat Acad Sci USA* **98**: 8133-8138.

Wan, A., Zhao, Z., Chen, X., He, Z., Jin, S., & Jia, Q., et al. (2004) Wheat stripe rust epidemic and virulence of *Puccinia striiformis* f. sp. *tritici* in China in 2002. *Plant Dis* **88**: 896-904.

Wang, C., Zhang, Y.P., Han, D.J., Kang, Z.S., Li, G.P., Cao, A.Z., and Chen, P.D. (2008) SSR and STS markers for wheat stripe rust resistance gene *Yr26*. *Euphytica* **159:** 359-366.

Wang, C.F., Huang, L.L., Buchenauer, H., Han, Q.M., Zhang, H.C., and Kang, Z.S. (2007) Histochemical studies on the accumulation of reactive oxygen species (O_2^- and H_2O_2) in the incompatible and compatible interaction of wheat-*Puccinia striiformis* f. sp *tritici*. *Physiol Mol Plant Pathol* **71**: 230-239.

Wang, C.F., Zhang, S.J., Hou, R., Zhao, Z.T., Zheng, Q., Xu, Q.J., *et al*. (2011) Functional analysis of the kinome of the wheat scab fungus *Fusarium*

graminearum. *PLoS Pathog* **7**: e1002460.

Wang, X., and McCallum, B. (2009) Fusion body formation, germ tube anastomosis, and nuclear migration during the germination of urediniospores of the wheat leaf rust fungus, *Puccinia triticina*. *Phytopathology* **99**: 1355-1364.

Yap, K.L., Kim, J., Truong, K., Sherman, M., Yuan, T., and Ikura, M. (2000) Calmodulin target database. *J Struct Funct Genomics* **1**: 8-14.

Yi, M., Park, J.H., Ahn, J.H., and Lee, Y.H. (2008) *MoSNF1* regulates sporulation and pathogenicity in the rice blast fungus *Magnaporthe oryzae*. *Fungal Genet Biol* **45**: 1172-1181.

Yin, C., Jurgenson, J.E., and Hulbert, S.H. (2011) Development of a host-induced RNAi system in the wheat stripe rust fungus *Puccinia striiformis* f. sp. *tritici*. *Mol Plant Microbe Interact* **24**: 554-561.

Yuan, S.M., Nie, W.C., He, F., Jia, Z.W., and Gao, X.D. (2016) Kin2, the budding yeast ortholog of animal MARK/PAR-1 kinases, localizes to the sites of polarized growth and may regulate septin organization and the cell wall. *PLoS ONE* **11**: e0153992.

Zaman, S., Lippman, S.I., Zhao, X., and Broach, J.R. (2008) How *Saccharomyces* responds to nutrients. *Annu Rev Genet* **42**: 27-81.

Zhang, H., Guo, J., Voegele, R.T., Zhang, J.S., Duan, Y.H., Luo, H.Y., and Kang, Z.S. (2012) Functional characterization of calcineurin homologs *PsCNA1/PsCNB1* in *Puccinia striiformis* f. sp *tritici* using a host-induced RNAi system. *PLoS ONE* **7**: e49262.

Zheng, W.M., Huang, L.L., Huang, J.Q., Wang, X.J., Chen, X.M., Zhao, J., *et al*. (2013) High genome heterozygosity and endemic genetic recombination in the wheat stripe rust fungus. *Nat Commun* **4**: 2673.

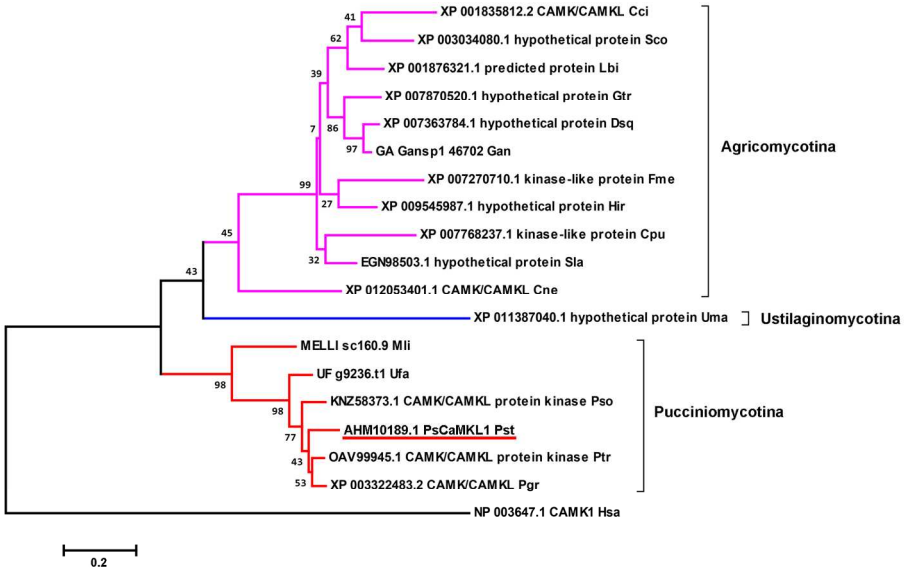

Fig. 1. Phylogeny of PsCaMKL1 and its orthologs. The phylogenetic tree was constructed with the Maximum-likelihood (ML) method using MEGA 7.0 software with 1,000 bootstrap values. CaMK1 from Homo sapiens is used as out-group. Branches are labeled with GenBank accession numbers and protein names. For abbreviations, see supporting information Table S1.

177x121mm (300 x 300 DPI)

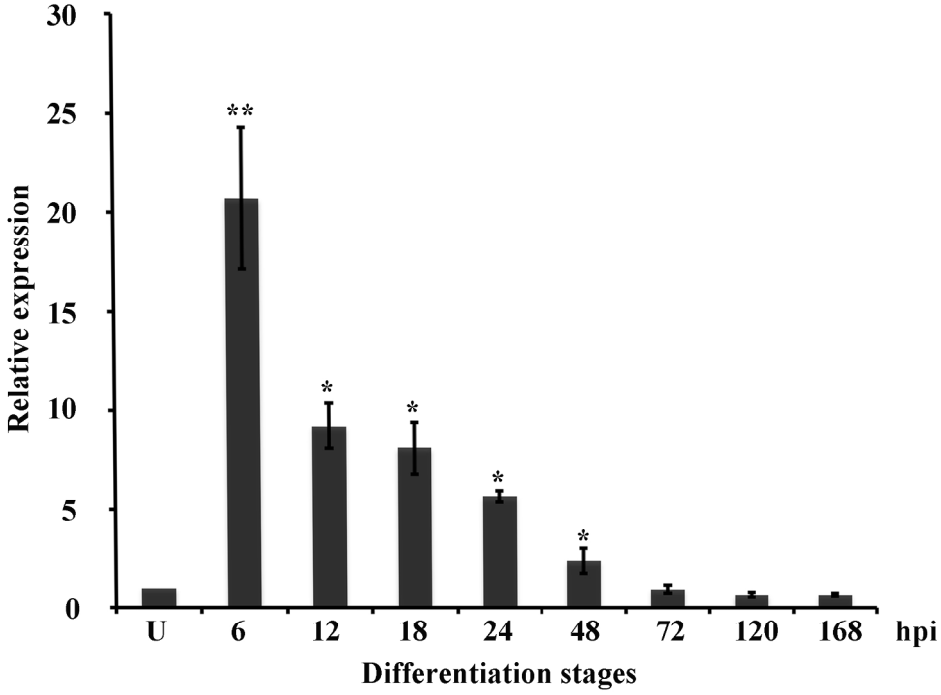

Fig. 2. Transcript profiles of PsCaMKL1 at different Pst infection stages. Transcript levels of PsCaMKL1 were calculated by the 2-ΔΔCT method with the elongation factor gene of Pst as endogenous reference. Values represent mean ± standard errors of three independent replicates. Differences were calculated by Student's t-tests. Asterisks indicate $P < 0.05$, double asterisks indicate $P < 0.01$. U, urediospores.

209x158mm (300 x 300 DPI)

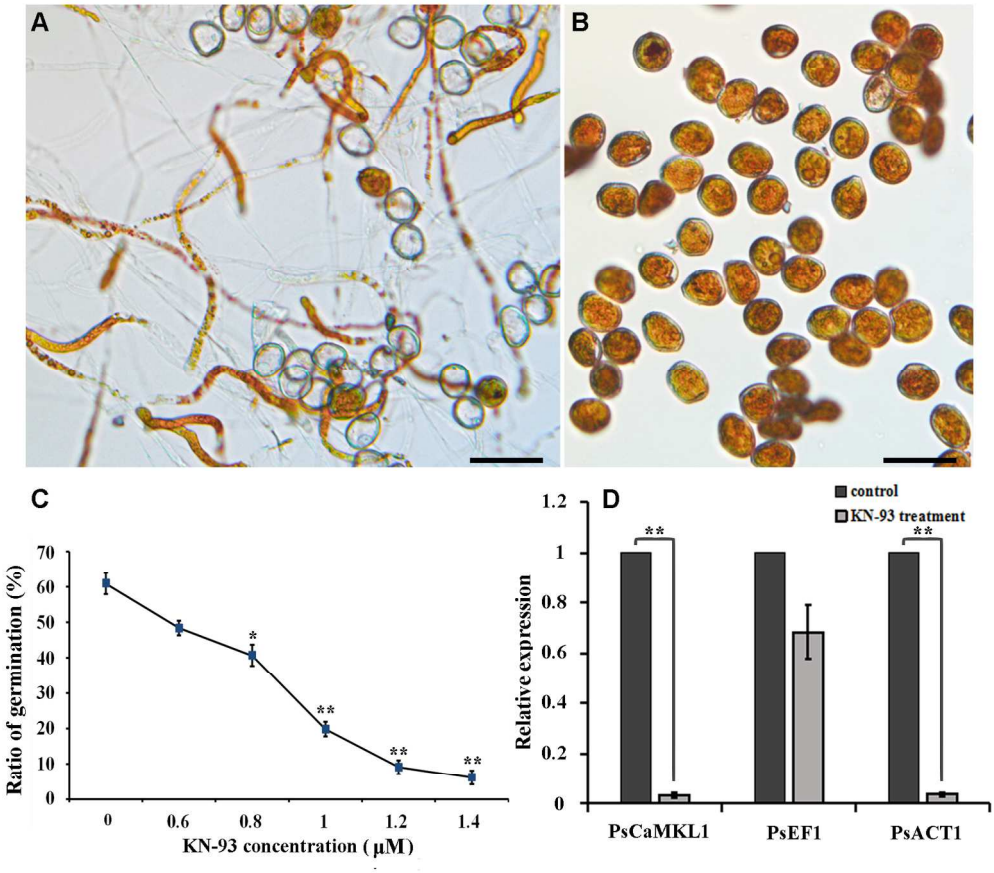

Fig. 3. Transcript levels of PsCaMKL1 were significantly decreased in barely germinated urediospores. (A) Germinated urediospores after 10 h treated with water (control). (B) Urediospores after 10 h treated with KN93 (1.4 μM). (C) The germination rate of Pst urediospores decreased gradually as KN93 concentration increased. (D) Transcript levels of PsCaMKL1 were significantly decreased in barely germinated urediospores at 6 hours post treatment with KN93 (1.4 μM). Values represent means ± standard errors of three independent replicates. Differences were calculated by Student's t-tests. Asterisks indicate $P < 0.05$ and double asterisks indicate $P < 0.01$.

164x149mm (300 x 300 DPI)

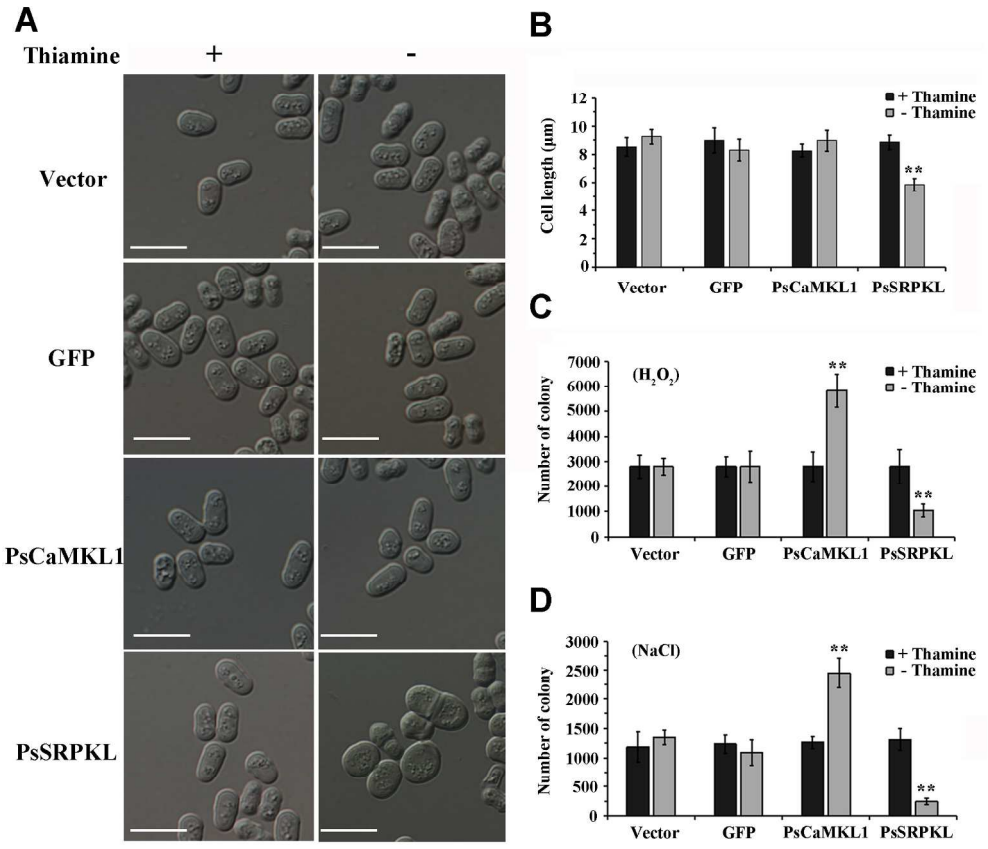

Fig. 4. Effects of overexpression of PsCaMKL1 in fission yeast. No significant morphological changes (A) and length change (B) were observed in PsCaMKL1-overexpressing yeast. Bars = 10 μm. The average number of growing yeast colonies under oxidative stress (C) and hyperosmotic stress (D) under inducing, or repressing conditions were calculated. Values represent means ± standard errors of three independent replicates. Differences were calculated by Student's t-tests. Double asterisks indicate $P < 0.01$.

209x184mm (300 x 300 DPI)

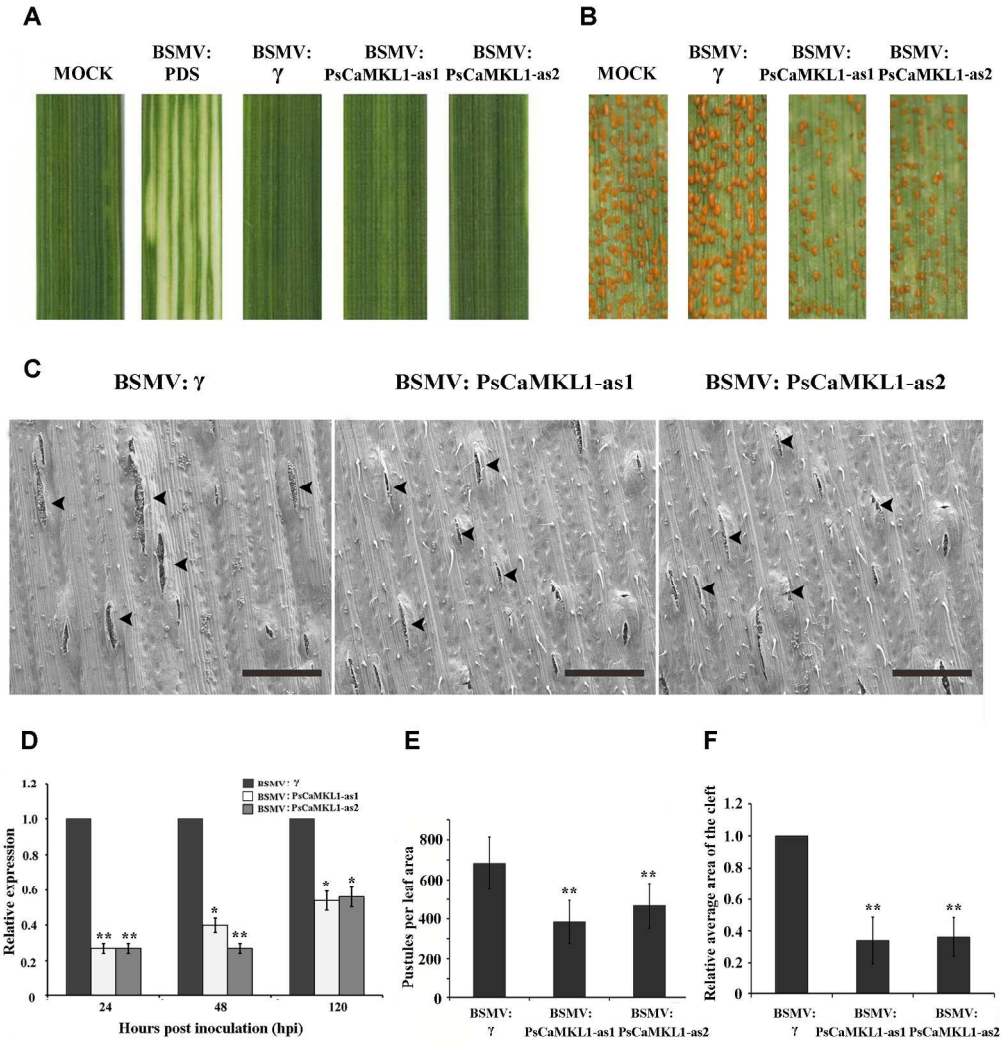

Fig. 5. Functional characterization of PsCaMKL1 using the BSMV-HIGS system. (A) Fourth leaves of plants with mild mosaic symptoms inoculated with buffer (mock), BSMV:PDS, BSMV:γ (vector control), BSMV:PsCaMKL1-as1, or BSMV:PsCaMKL1-as2 at 10 dpi. BSMV:TaPDS exhibits the expected photo-bleaching phenotype. (B) Phenotypes of the fourth leaves inoculated with buffer (mock), BSMV:γ (empty vector), PsCaMKL1-as1, or BSMV:PsCaMKL1-as2 14 dpi with the virulent Pst isolate CYR32. (C) Observation of the clefts on the fourth leaves of wheat plants inoculated with BSMV:γ, BSMV:PsCaMKL1-as1, or BSMV:PsCaMKL1-as2 at 14 dpi with the virulent Pst isolate CYR32 under the scanning electron microscope. Bars = 500 μm. (D) Relative transcript abundance of PsCaMKL1 in knock-down wheat leaves. RNA samples were isolated from the fourth leaves of wheat infected with BSMV:γ, BSMV:PsCaMKL1-as1, or BSMV:PsCaMKL1-as2 at 24, 48 and 168 hpi with the CYR32 isolate. Values are expressed relative to an endogenous Pst reference gene EF1, with the empty vector (BSMV:γ) set at 1. (E) Quantification of the density of Pst urediospores in silenced plants 14 dpi with the CYR32 isolate. (F) Quantification of the relative average area of the cleft in silenced plants 14 dpi with the CYR32 isolate. Values represent means ± standard errors of three independent samples. Differences were assessed using Student's t-tests. Asterisks indicate $P < 0.05$ and double asterisks indicate $P < 0.01$.

209x230mm (300 x 300 DPI)

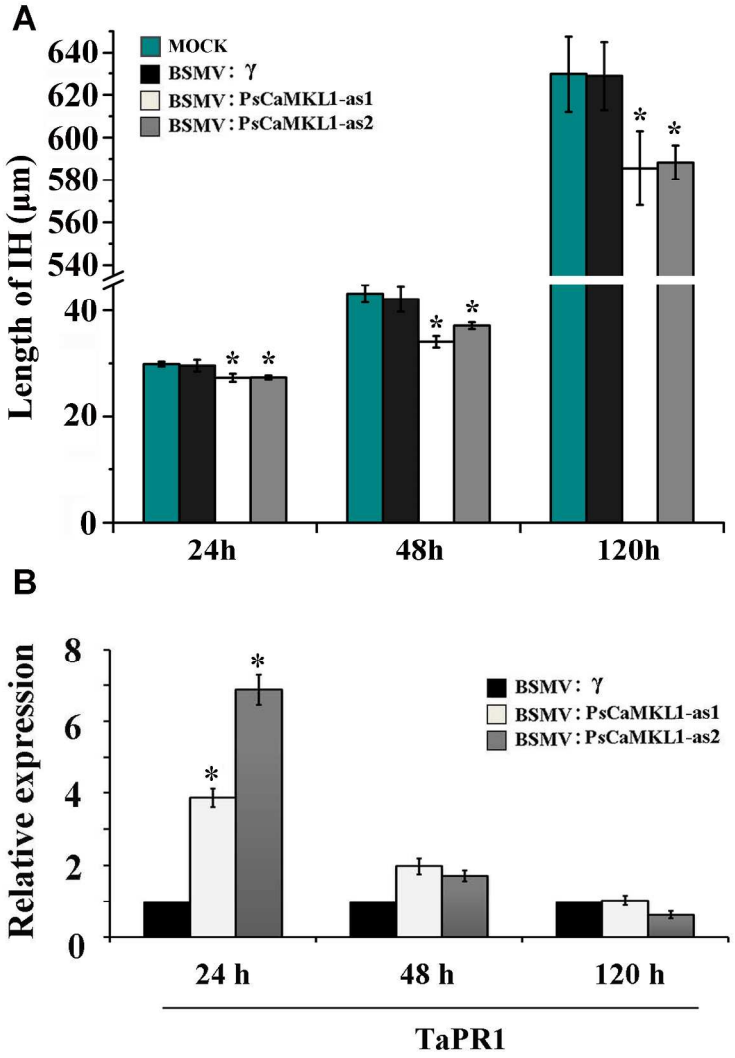

Fig. 6. HIGS of PsCaMKL1 shows compromised fungal development in wheat cells. HIGS of PsCaMKL1 showed significantly decreased hyphal length at 24, 48 and 120 hpi. (A) Hyphal length was the average distance of the longest hypha from the origin on the substomatal vesicle (SV) to the hyphal apex; measurement was done on DP-BSW software. (B) Transcript levels of TaPR1 (GenBank: KR351308.1) in PsCaMKL1-knockdown compared to control plants. Values represent means ± standard errors of three independent samples. Differences were assessed using Student's t-tests. Asterisks indicate $P < 0.05$.

209x297mm (300 x 300 DPI)

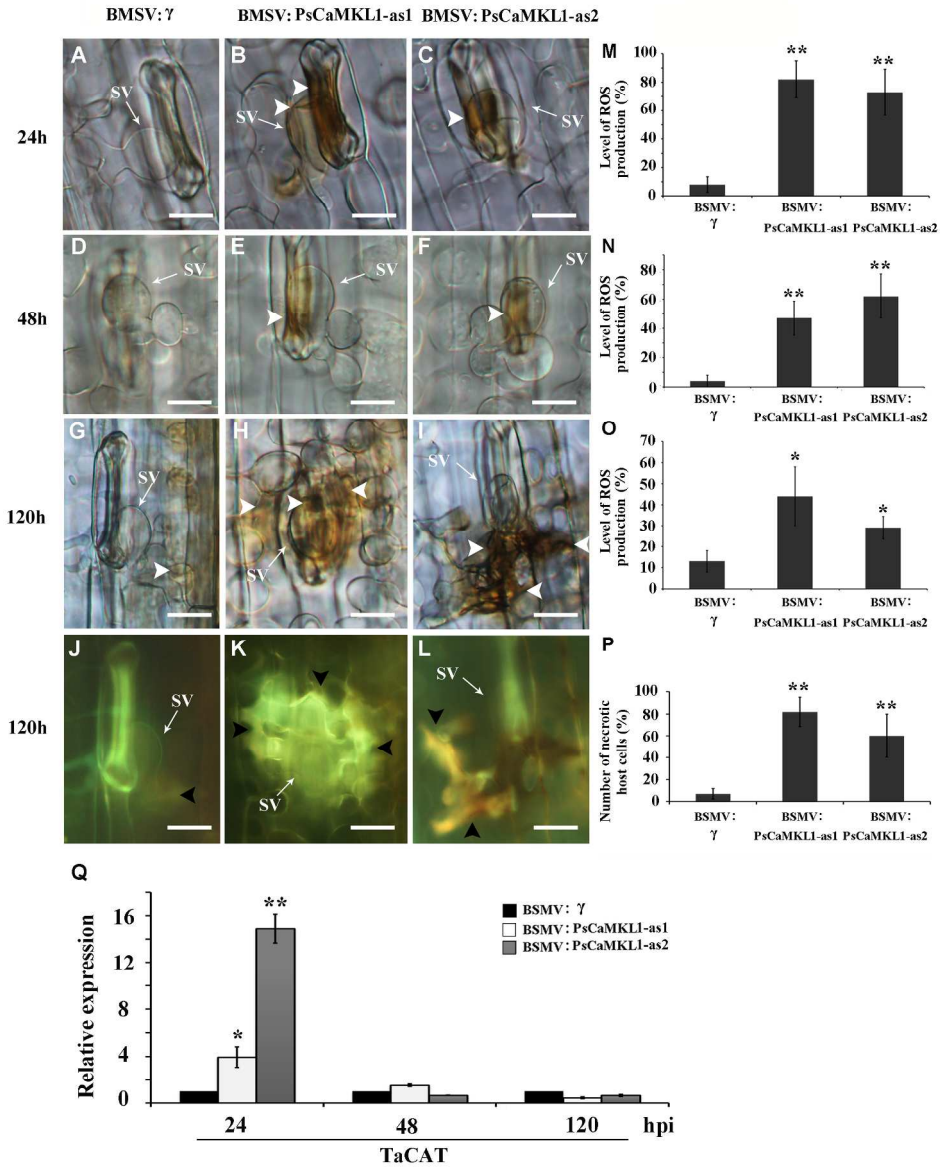

Fig. 7. Production of H2O2 and hypersensitive cell death in control and PsCaMKL1-silenced plants challenged with CYR32. H2O2 production was observed by DAB staining. Cell death was detected as autofluorescence. (A-I) Histological observation of the host response in wheat infected with BSMV:γ, or recombinant BSMV after inoculation with CYR32. H2O2 accumulation at 24 hpi (A-C), 48 hpi (D-F), and 120 hpi (G-I) in BSMV:γ, BSMV:PsCaMKL1-as1, or BSMV:PsCaMKL1-as2 infected plants. (J-L) Hypersensitive cell death at 120 hpi in BSMV:γ, BSMV:PsCaMKL1-as1, or BSMV:PsCaMKL1-as2 infected plants. (M-P) Level of ROS production and infection site with necrotic cells in wheat infected by BSMV:γ, or recombinant BSMV after inoculation with CYR32. Level of ROS production at 24 hpi (M), 48 hpi (N) and 120 hpi (O) in BSMV:γ, BSMV:PsCaMKL1-as1, or BSMV:PsCaMKL1-as2 infected plants. Number of infection sites with necrotic cells at 120 hpi (P) in BSMV:γ, BSMV:PsCaMKL1-as1, or BSMV:PsCaMKL1-as2 infected plants. White arrowheads show the position of H2O2 accumulation. Black arrowheads show the position of necrotic cells. Bars = 20 μm. (Q) Transcript levels of TaCAT (GenBank: X94352.1) in PsCaMKL1-knockdown compared to control plants. Values represent means ± standard errors of three independent replicates. Differences were

calculated by Student's t-tests. Asterisks indicate P < 0.05 and double asterisks indicate P < 0.01.

209x263mm (300 x 300 DPI)